

Revised immunolocalization of the Na⁺-D-glucose cotransporter SGLT1 in rat organs with an improved antibody

Daniela Balen, Marija Ljubojevic, Davorka Breljak, Hrvoje Brzica, Vilim Zlender, Hermann Koepsell and Ivan Sabolic

Am J Physiol Cell Physiol 295:475-489, 2008. First published Jun 4, 2008;
doi:10.1152/ajpcell.00180.2008

You might find this additional information useful...

This article cites 60 articles, 31 of which you can access free at:

<http://ajpcell.physiology.org/cgi/content/full/295/2/C475#BIBL>

Updated information and services including high-resolution figures, can be found at:

<http://ajpcell.physiology.org/cgi/content/full/295/2/C475>

Additional material and information about *AJP - Cell Physiology* can be found at:

<http://www.the-aps.org/publications/ajpcell>

This information is current as of August 13, 2008 .

Revised immunolocalization of the Na⁺-D-glucose cotransporter SGLT1 in rat organs with an improved antibody

Daniela Balen,¹ Marija Ljubojević,¹ Davorka Breljak,¹ Hrvoje Brzica,¹ Vilim Žlender,¹ Hermann Koepsell,² and Ivan Sabolić¹

¹Molecular Toxicology, Institute for Medical Research and Occupational Health, Zagreb, Croatia; and ²Anatomy and Cell Biology, University of Würzburg, Würzburg, Germany

Submitted 28 March 2008; accepted in final form 28 May 2008

Balen D, Ljubojević M, Breljak D, Brzica H, Žlender V, Koepsell H, Sabolić I. Revised immunolocalization of the Na⁺-D-glucose cotransporter SGLT1 in rat organs with an improved antibody. *Am J Physiol Cell Physiol* 295: C475–C489, 2008. First published June 4, 2008; doi:10.1152/ajpcell.00180.2008.—Previously, we characterized localization of Na⁺-glucose cotransporter SGLT1 (*Slc5a1*) in the rat kidney using a polyclonal antibody against the synthetic COOH-terminal peptide of the rat protein (Sabolić I, Škarica M, Gorboulev V, Ljubojević M, Balen D, Herak-Kramberger CM, Koepsell H. *Am J Physiol Renal Physiol* 290: 913–926, 2006). However, the antibody gave some false-positive reactions in immunochemical studies. Using a shortened peptide for immunization, we have presently generated an improved, more specific anti-rat SGLT1 antibody (rSGLT1-ab), which in immunochemical studies with isolated membranes and tissue cryosections from male (M) and female (F) rats exhibited 1) in kidneys and small intestine, labeling of a major protein band of ~75 kDa; 2) in kidneys of adult animals, localization of rSGLT1 to the proximal tubule (PT) brush-border membrane (S1 < S2 < S3) and intracellular organelles (S1 > S2 > S3), with zonal (cortex < outer stripe) and sex differences (M < F) in the protein expression, which correlated well with the tissue expression of its mRNA in RT-PCR studies; 3) in kidneys of castrated adult M rats, upregulation of the protein expression; 4) in kidneys of prepubertal rats, weak and sex-independent labeling of the 75-kDa protein band and immunostaining intensity; 5) in small intestine, sex-independent regional differences in protein abundance (jejunum > duodenum = ileum); and 6) thus far unrecognized localization of the transporter in cortical thick ascending limbs of Henle and macula densa in kidney, bile ducts in liver, enteroendocrine cells and myenteric plexus in the small intestine, and initial ducts in the submandibular gland. Our improved rSGLT1-ab may be used to identify novel sites of SGLT1 localization and thus unravel additional physiological functions of this transporter in rat organs.

brain; enteroendocrine cells; sex differences; kidney; liver; myenteric plexus; proximal tubule; salivary gland; small intestine

IN THE MAMMALIAN KIDNEY, the low-affinity/high-capacity Na⁺-glucose cotransporter SGLT2 (*Slc5a2*) mediates bulk of glucose reabsorption in the early part of proximal convoluted tubule, whereas the high-affinity/low-capacity SGLT1 (*Slc5a1*) in the distal part of proximal tubule reduces intraluminal glucose to very low levels (59, 60). Possible functions of the third member of SGLT family, SGLT3 (*Slc5a4*; isoforms A and B), as the glucose sensor and/or transporter, as well as its intrarenal distribution have not been resolved (14, 59). At the protein level, the two major brush-border glucose transporters in the proximal tubules differ in their affinity for glucose and

Na⁺ (SGLT1 > SGLT2), selectivity of sugars (SGLT2 transport glucose at least 10 times better, whereas SGLT1 transports glucose and galactose equally well), and sensitivity to inhibitor phlorizin (SGLT1 > SGLT2). Both SGLTs have ~660 amino acid residues that share 59% homology and may function as glycosylated monomers of 70–80 kDa (18, 26, 28, 50, 52, 58, 59).

Transport and mRNA studies in isolated nephron segments and membrane vesicles from various tissue zones of the rat and rabbit kidneys have indicated segmental and zonal differences in the expression of two major SGLTs; SGLT2 was largely localized to the proximal tubule S1 and S2 segments in the cortex, whereas SGLT1 was localized more to the proximal tubule S3 segments in the medullary rays and outer stripe (3, 34, 45, 54–56, 60). However, the exact immunolocalization of these transporters and the level of their expression along the renal nephron are not entirely clear due to the lack of specific antibodies. Several polyclonal anti-peptide antibodies have been raised against SGLT1 that recognize proteins in the brush border of rat and rabbit small intestine and renal tubules; in kidney, the transporter protein was localized to either the entire proximal tubule or more abundantly to the tubules of renal outer medulla (10, 29, 45, 50, 52).

In our recent studies, we used a polyclonal antibody against the synthetic COOH-terminal peptide of the rat SGLT1 (rSGLT1-ab), generated by us, which in rats immunostained the apical domain of small intestine and endothelial cells in capillaries of the brain, skeletal, and heart muscles (17, 18), whereas in rat and mouse kidneys, this antibody stained with varying intensity brush border along the entire proximal tubule, exhibiting zonal differences due to segmental heterogeneity (S1 = S2 < S3) and female-dominant sex differences in staining intensity (50). However, in the latter study, it turned out that the antibody also stained the walls of small and large arteries, basolateral and apical membranes of distal tubules and collecting ducts, and smooth muscles in the renal capsule and external blood vessels, whereas in Western blots of isolated renal membranes, in addition to the rSGLT1-related ~75-kDa protein band, it strongly labeled the 40-kDa protein band. Because both bands were blocked by the immunizing peptide and followed the same labeling/staining pattern in various immunochemical experiments, the 40-kDa band has been considered as the splitting product of the 75-kDa band. However, using the database search program BLAST, we have compared the amino acid sequence of our old rSGLT1-peptide with the sequences of

Address for reprint requests and other correspondence: I. Sabolić, Molecular Toxicology, Institute for Medical Research and Occupational Health, Ksaverska cesta 2, HR-10001 Zagreb, Croatia (e-mail: sabolic@imi.hr).

The costs of publication of this article were defrayed in part by the payment of page charges. The article must therefore be hereby marked “advertisement” in accordance with 18 U.S.C. Section 1734 solely to indicate this fact.

other proteins and detected a limited similarity with relevant sequences in the two members of Coxsackie- and adenovirus receptor-like membrane proteins (CAR-LMP) that reside in junctional complexes between endothelial or epithelial cells and seem to participate in cell-cell adhesion (16, 48, 50). Our old rSGLT1 antibody was generated 2 yr before the sequences of CAR-LMP were published, and this limited similarity could not be recognized earlier. By following the search data, the critical common three-amino acid residues in the old synthetic peptide have been removed, and a new polyclonal antibody against the shorter peptide has been generated. As shown in this report, the new antibody proved to be more specific for rSGLT1 in both immunoblotting and immunocytochemical studies.

MATERIALS AND METHODS

Animals and treatment. Adult (10–12 wk old) and prepubertal (25 days old) male and female Wistar strain rats were from the breeding colony at the Institute in Zagreb. Animals were bred and maintained according to the “Guide for the Care and Use of Laboratory Animals” [DHEW Publication No. (NIH) 85-23, Revised 1996, Office of Science and Health Reports, DRR/NIH, Bethesda, MD 20205]. Before and during experiments, animals had free access to standard pelleted food (diet 4RF21; Mucedola, Settimo Milanese, Italy) and tap water. The studies were approved by the Institutional Ethic Committee.

Gonadectomy was performed on the adult animals. Male rats were castrated by scrotal route, whereas female rats were ovariectomized by dorsal (lumbar) approach under proper anesthesia (Narketan, 80 mg/kg body mass-Xylapan, 12 mg/kg body mass ip). The sham-operated animals underwent the same procedure but without removal of the organs.

Antibodies and other material. Polyclonal immune serum against the peptide specific for the COOH-terminal sequence of rSGLT1 (PKDTIEIDAEAPQKEK, amino acids 585–600) was raised in rabbits. This 16-meric peptide was shorter by 3 amino acids in the rSGLT1 COOH-terminal domain (EED, amino acids 582–584) than the peptide used in our previous antibody production (17, 18). The novel rSGLT1-ab was affinity-purified from the immune serum via the antigenic peptide-coupled support on a column (17). The eluates with the highest titers were used for immunocytochemical studies, whereas the eluates with lower titers were used for Western blotting. The use of polyclonal anti- Na^+/K^+ -ATPase α -subunit antibody (Na/K-ATPase-ab) and commercially available monoclonal anti- α -actin antibody (α -actin-ab) (Chemicon International, Temecula, CA) has been described previously (2, 11, 50). Secondary antibodies were purchased commercially from Jackson ImmunoResearch Laboratories (West Grove, PA) or Kirkegaard and Perry (Gaithersburg, MD) and included the CY3-labeled (GARCY3) or FITC-labeled (GARF) goat anti-rabbit IgG or alkaline phosphatase-labeled goat anti-rabbit (GARAP) or goat anti-mouse (GAMAP) IgG.

Anesthetics (Narketan and Xylapan) were purchased from Chassot (Bern, Switzerland); the molecular weight standards were obtained from Bio-Rad (Hercules, CA); and inhibitors (PMSF, antipain, and benzamidine) were purchased from Sigma (St. Louis, MO). All other chemicals and reagents were analytical grade and obtained from commercial sources such as Sigma or Fisher Scientific (Pittsburgh, PA). The sources of specific reagents and equipment for Western blotting, immunocytochemistry, RNA isolation, and end-point RT-PCR assay are indicated in the text related to these methods.

Tissue fixation and immunocytochemistry. In adult rats, various organs were fixed by perfusion *in vivo* (36, 37, 50). The circulatory system of anesthetized animals was perfused via the left ventricle of the heart, using the Masterflex pump (Cole-Parmer, Chicago, IL), first with aerated (95% O_2 -5% CO_2) and temperature-equilibrated (37°C) phosphate-buffered saline (PBS; in mM: 137 NaCl, 2.7 KCl, 8

Na_2HPO_4 , and 2 K_2PO_4 , pH 7.4) for 2–3 min (to remove blood via the incised abdominal vena cava) and then with 150 ml of fixative (4% paraformaldehyde in PBS) for 4–5 min. The organs (kidneys, small intestine, brains, liver, submandibular glands, heart, and skeletal muscle) were removed, sliced, and kept overnight in the same fixative at 4°C, followed by extensive washing in PBS and storage in PBS containing 0.02% NaN_3 at 4°C until further use. Prepubertal rats were killed by cervical dislocation, the abdominal cavity was opened, and the kidneys were removed, rinsed with ice-cold PBS, sliced, put in a fixative, and further processed as described for tissue slices from adult rats.

To cut 4- μm frozen sections, tissue slices were infiltrated with 30% sucrose (in PBS) overnight, embedded in OCT medium (Tissue-Tek, Sakura, Japan), frozen at -25°C , and sectioned in a Leica CM 1850 cryostat (Leica instruments, Nussloch, Germany). Sections were collected on Superfrost/Plus microscope slides (Fischer Scientific), dried at room temperature for 2–3 h, and kept refrigerated until further use.

Before the primary antibody was applied, cryosections underwent an antigen retrieval procedure to expose cryptic antibody binding sites. The following consecutive steps were used: 1) rehydration in PBS for 15 min; 2) heating in 10 mM citrate buffer, pH 6, for 20 min in a microwave oven (4 cycles, 5 min each at 800 W); after each cycle, the level of buffer was checked and the evaporated amount replenished; 3) cooling down to room temperature in the same buffer for 20 min; 4) rinsing in PBS (3 times, 5 min each); 5) incubation in 0.5% Triton X-100 (in PBS) for 15 min; 6) incubation in 2% Triton X-100 (in PBS) for 30 min; 7) rinsing in PBS (3 times, 5 min); 8) incubation in bovine serum albumin (1% BSA in PBS; to block the nonspecific antibody binding) for 30 min; 9) incubation with the old (diluted 1:50 with PBS) (50) or new rSGLT1-ab (diluted 1:2,000–1:500 in PBS) overnight (10–12 h) in a refrigerator; 10) incubation in 0.1% Triton X-100 (in PBS) for 10 min; 11) rinsing in PBS (2 times, 5 min); 12) incubation with GARCY3 (1.6 $\mu\text{g}/\text{ml}$ in PBS) or GARF (15 $\mu\text{g}/\text{ml}$) at room temperature for 60 min; 13) incubation in 0.1% Triton X-100 (in PBS) for 10 min; 14) rinsing in PBS (2 times, 5 min); and 15) mounting in a fluorescence fading retardant (Vectashield; Vector Laboratories, Burlingame, CA).

To costain rSGLT1 and Na^+/K^+ -ATPase with their specific (both polyclonal) antibodies, we had to adapt incubation times with the secondary antibodies; the adaptations were optimized in preliminary experiments (data not shown). Shortly, cryosections were incubated with the first primary antibody overnight and then with the first secondary antibody for 2 h at room temperature to saturate the primary antibody-related binding sites. Next followed incubation with the second primary antibody overnight and then with the second secondary antibody for only 20 min to diminish labeling by the first primary antibody. Thus, in one approach, sections were incubated (in sequence) with the rSGLT1-ab (1:1,000) in a refrigerator overnight, rinsed with 0.1% Triton X-100 and PBS as described above, incubated with GARCY3 at room temperature for 2 h, rinsed with 0.1% Triton X-100 and PBS, incubated with the Na/K-ATPase-ab (1:50) in a refrigerator overnight, rinsed with 0.1% Triton X-100 and PBS, incubated with GARF (15 $\mu\text{g}/\text{ml}$ in PBS) at room temperature for 20 min, and rinsed with 0.1% Triton X-100 and PBS. In another approach, the sequence of primary and secondary antibodies was reversed, e.g., the Na/K-ATPase-ab was applied first overnight, followed by GARCY3 at room temperature for 2 h, and then rSGLT1-ab was applied overnight, followed by GARF for 20 min at room temperature. Either way, the sections were finally covered with Vectashield and prepared for microscopy.

To test the staining specificity, we performed the following steps: 1) rSGLT1-ab was blocked with the immunizing peptide (final concentration of peptide: 0.5 mg/ml) for 4 h at room temperature before use in the above-described immunofluorescence assay; 2) the rSGLT1-ab-related immunostaining was tested in the organs in which the presence of SGLT1 was not to be expected (stomach, colon); and 3) tissue sections were incubated with the secondary antibodies only.

The stained sections were examined and photographed with an Opton III RS fluorescence microscope (Opton Feintechnik, Oberkochen, Germany) using a Spot RT Slider camera and software (Diagnostic Instruments, Sterling Heights, MI). The images of CY3-related red fluorescence and FITC-related green fluorescence were taken separately using specific cut-off filters with no bleed-through effects. The images were imported into Adobe Photoshop 6.0 for processing, assembling, and labeling. Using the same software, we converted most CY3-related images into black-and-white mode, whereas the separate red and green images from double-staining experiments were adequately merged. The images were then assembled in panels and labeled.

Preparation of tissue homogenates and membranes. Animals were killed by decapitation. Kidneys were removed and either used in toto or sagittally sliced. From the slices, the cortex and outer stripe were dissected manually and used as separate tissue pools, whereas the inner stripe and inner medulla were processed as a single sample. The small intestine (mucosa scraped separately from duodenum, jejunum, and ileum), hearts, skeletal muscles, salivary glands, livers, brains, and abdominal aortas collected from four male and four female rats were processed as separate tissue pools. The details of tissue homogenization and differential centrifugation of the homogenates in refrigerated centrifuges were described previously (36, 37, 50). Total cell membranes (TCM) were collected as the pellet between 6,000 and 150,000 *g*. Brush-border membranes (BBM) from the renal (whole kidney, cortex, and outer stripe) and small intestinal mucosal tissue (duodenum, jejunum, and ileum) were isolated using the Mg²⁺-EGTA precipitation method (4). The final membrane preparations were resuspended in buffer that contained (in mM) 150 mannitol, 2.5 EGTA, and 12 Tris·HCl, pH 7.4, and were stored at -70°C until further use for immunoblotting studies. The protein was measured using the Bradford assay (5).

SDS-PAGE and Western blotting. If not stated differently, the preparation of membrane samples in Laemmli buffer [without β-mercaptoethanol (β-ME)], denaturation at 65°C for 15 min, and separation of the proteins through 10% SDS-PAGE mini gels, as well as electrophoretic wet-transfer to an Immobilon membrane (Millipore, Bedford, MA), were performed exactly as described previously (50). The amount of protein per lane in SDS-PAGE is as indicated. The transfer membrane was blocked in blotting buffer (5% nonfat dry milk, 0.15 M NaCl, 1% Triton X-100, and 20 mM Tris·HCl, pH 7.4) and incubated at 4°C overnight (12–14 h) in the same buffer containing our old (50) or new rSGLT1-ab (1:1,000) or α-actin-ab (0.5 μg/ml). The membrane was then washed four times for 15 min with blotting buffer, incubated for 60 min in the same buffer that contained either 0.1 μg/ml GARAP or 0.5 μg/ml GAMAP, washed again, and stained for alkaline phosphatase activity using the BCIP/NBT [5-bromo-4-chloro-3-indolyl phosphate (1.65 mg/ml)/nitroblue tetrazolium (3.3 mg/ml) in 20 mM Tris·HCl buffer, pH 9.0] method as an indicator. The labeled protein bands were evaluated using densitometry; the quantification was performed using the Quantity One 1-D analysis software (Bio-Rad Laboratories) after marking an area of the broadest 75-kDa protein band in the blot, and an equal area was applied to all other bands in the same blot. The area density of each band was expressed in arbitrary units relative to the strongest band density (1 unit) in the corresponding control samples. In preliminary

experiments, with the use of isolated BBM from the outer stripe of male and female kidneys and isolated BBM from the male duodenum and jejunum, the density of the 75-kDa protein band was approximately linear between 20 and 80 μg protein/lane (data not shown). Our experiments were performed using the amounts of protein per lane within the linear range of band density. To demonstrate specific labeling, rSGLT1-ab was preincubated with the immunizing peptide (final concentration of peptide: 0.5 mg/ml) for 4 h at room temperature and then used in an immunoblotting assay as described above.

Isolation of RNA and end-point RT-PCR. The animals were killed by decapitation. The kidneys were removed, decapsulated, and cut into 1-mm-thick sagittal slices, and one slice was immediately submerged into the RNAlater solution (Sigma). Cortical and outer stripe tissues were manually separated, and total cellular RNA from these zones was extracted using Trizol according to the manufacturer's instructions (Invitrogen, Carlsbad, CA). RNA concentration and purity were estimated by spectrophotometric measurement of the optical density at 260/280 nm. The quality and integrity of RNAs were tested by agarose gel electrophoresis. Isolated preparations of RNA were stored at -70°C until use.

The first-strand cDNA synthesis was performed using the First-Strand cDNA synthesis kit following the prescribed instructions (Fermentas International, Burlington, ON, Canada). Isolated RNA (3 μg) was denatured at 70°C for 5 min in reaction mixture containing 0.5 μg of oligo(dT)₁₈ and then reverse transcribed in a total volume of 20 μl of reaction mixture containing 1× reverse transcription buffer, 20 units of ribonuclease inhibitor, 1 mM dNTP mix, and 40 units of Moloney murine leukemia virus reverse transcriptase. This mixture was incubated first at 37°C for 60 min and then at 72°C for 10 min. The generated cDNAs were diluted 5× in DNase/RNase-free water (GIBCO/Invitrogen), and stored at -20°C until use. PCR was performed in a total volume of 20 μl using 1 μl of 5× diluted first-strand cDNA, 0.4 μM rSGLT1-specific primers (Invitrogen Online), and ready-to-use PCR Master Mix (Applied Biosystems, Foster City, CA) following the manufacturer's instructions. The housekeeping gene β-actin was used as a control for variations in the input of RNA. For PCR, the sequences of specific forward and reverse rSGLT1 and β-actin intron over-spanning primers, custom purchased from Invitrogen Online, were used to avoid amplification of genomic DNA (Table 1). The PCR conditions were as follows: initial denaturation for 3 min at 94°C, denaturation for 30 s at 95°C, annealing for 30 s at 59°C, and elongation for 45 s at 72°C, with 30 cycles for both rSGLT1 and β-actin. The optimal number of PCR cycles within the exponential phase of the PCR reaction was determined in preliminary experiments (data not shown). In each PCR, nontemplate control reactions (cDNA was substituted with DNase/RNase-free water) were also included, but no PCR products were detected, indicating the absence of possible contamination (data not shown). RT-PCR products were resolved by electrophoresis in 1% agarose gel, stained with ethidium bromide, visualized under ultraviolet light, and photographed with a digital camera, and images were imported into Adobe Photoshop 6.0 for processing and labeling.

Presentation of data. The immunocytochemical data represent findings in three to four animals in each experimental group; the immunoblotting studies were performed with four to six independent BBM or TCM preparations in each experimental group, whereas

Table 1. Primer sequences used for end-point RT-PCR

Gene	Forward (f)/Reverse (r) Primers (5'-3')	GenBank Accession No.	Location	PCR Product Size, bp
rSGLT1	f: ATTCATCAATCTGGCCTTGG r: TATTCGGAGACCCCATACG	NM_013033	628–648 920–940	313
β-Actin	f: GTCGTACCACTGGCATTGTG r: AGGAAGGAAGGCTGGAAGAG	NM_031144	518–537 862–881	364

rSGLT1, rat Na⁺-glucose cotransporter 1.

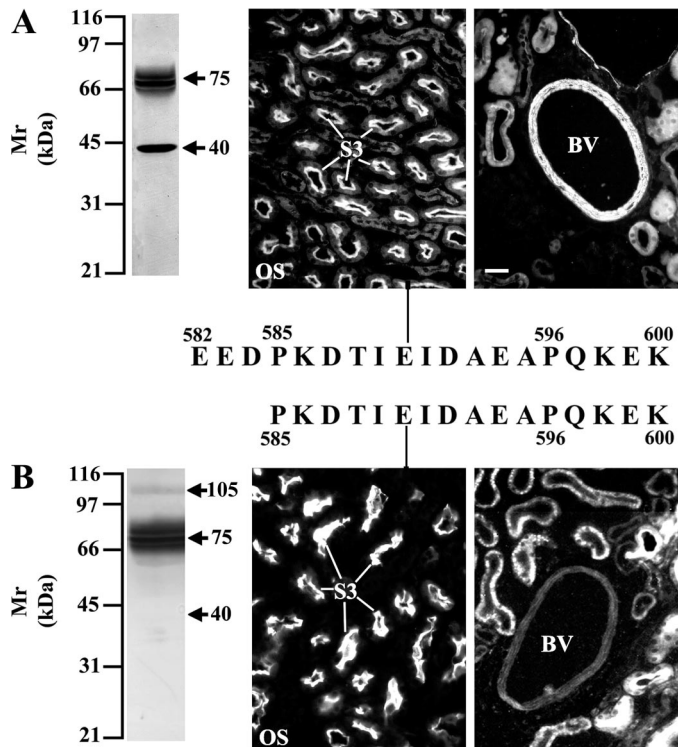


Fig. 1. Immunocytochemical characterization of our old anti-rat Na⁺-glucose cotransporter SGLT1 antibody (rSGLT1-ab), which was generated against the 19-mer peptide and used in our previous studies (17, 18, 50), and of the new antibody, which was generated against a peptide shorter by the 3 initial amino acid residues (EED) and used in the present study. *A*: the old antibody strongly labeled the ~40- and ~75-kDa protein bands in Western blotting of brush-border membrane (BBM) isolated from the renal outer stripe (OS) and stained the BBM of proximal tubule S3 segments in the OS and smooth muscles of the renal blood vessels (BV) by immunocytochemistry. *B*: the novel rSGLT1-ab labeled strongly the protein band of ~75-kDa and faintly the band of ~105-kDa in Western blotting of BBM and strongly stained the BBM of S3 segments in the OS, whereas the BV remained unstained. The immunoblots were performed with 60 µg of protein per lane. Mr, molecular mass. Bar, 20 µm.

RT-PCR studies were performed with two independent RNA preparations from the male and female kidney cortex and outer stripe. The numeric data, expressed as means ± SE, were statistically evaluated using Student's *t*-test and either ANOVA or Duncan's test at the 5% level of significance.

RESULTS

Comparison of our old and new rSGLT1-ab in immunocytochemical studies. Previously, we described localization and sex differences of rSGLT1 in rat kidney and a few other organs using an antibody generated against the 19-meric peptide identical to rSGLT1 COOH-terminal domain. However, it turned out that this antibody exhibited nonspecific immunocytochemical reactions in tissue cryosections of various organs that could not be suppressed reliably, as assumed in the first experiments (17, 18, 50). After performing the proper search of amino acid sequences in the rSGLT1 peptide and in homologous peptides from the relevant non-rSGLT1 proteins (BLASTP 2.2.10; National Center for Biotechnology Information, NCBI Sequence Viewer FASTA; National Library of Medicine, Bethesda, MD), from the previous 19-meric peptide we removed 3 initial amino acids (EED) common to CAR-

LMP and used a shorter, 16-meric peptide for generating the novel, more specific rSGLT1-ab in rabbits.

In Fig. 1, we compared immunocytochemical potency of the old (A) and novel rSGLT1-ab (B). In accordance with our previous data (50), in Western blot of isolated renal BBM from the outer stripe, the old antibody strongly labeled two protein bands, one at ~40 kDa and another at ~75 kDa, and by immunocytochemistry it stained not only the BBM of proximal tubule S3 segments in the outer stripe and smooth muscles of the renal blood vessels (Fig. 1A) but also capillary epithelium and various other structures in kidney and other organs (not shown). However, the novel rSGLT1-ab in the same membrane preparation labeled strongly the rSGLT1-related protein band

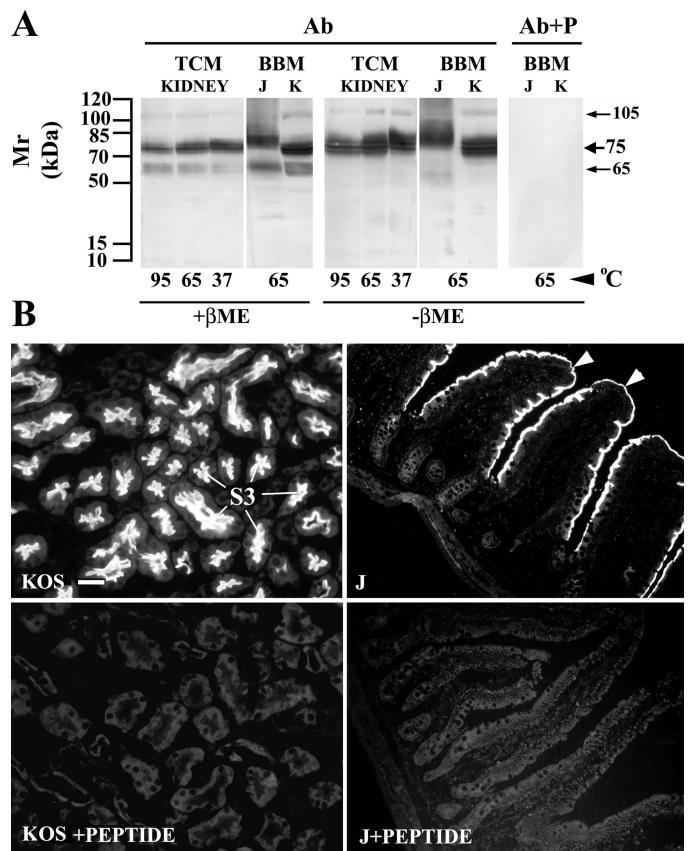


Fig. 2. Immunocytochemical characterization of the new rSGLT1-ab. *A*: testing optimal immunoblotting conditions in total cell membrane (TCM) and BBM from the female kidney OS (K) and in BBM from the female jejunum (J). Isolated membranes were incubated in Laemmli buffer with (+β-ME) or without β-mercaptoethanol (-β-ME) at the indicated temperatures for 5 min (95°C), 15 min (65°C), or 30 min (37°C) and blotted with intact (Ab) or peptide-blocked (Ab+P) antibody. In the presence of β-ME, in kidney membranes, the antibody labeled 3 protein bands of ~65 (weak), ~75 (strong), and ~105 kDa (faint), whereas in the jejunal BBM, the antibody labeled bands of ~65 (weak) and ~80 kDa (strong). In the absence of β-ME, in renal TCM and BBM preparations, the ~65-kDa band was absent, the ~75-kDa band was faint and strongly labeled, and the ~105-kDa band was faintly labeled, whereas in the jejunal BBM, only one faint band of ~80 kDa was labeled. In optimal conditions (-β-ME, 65°C, 15 min), the bands in BBM from both tissues were blocked after preincubation of the antibody with the immunizing peptide (Ab+P). Each lane contained 40 (BBM) or 60 (TCM) µg of protein. *B*: in optimal conditions in tissue cryosections, the antibody strongly stained the brush border of proximal tubule S3 segments in the kidney OS (KOS) and jejunum (J). This staining was abolished after preincubation of the antibody with the immunizing peptide (KOS+PEPTIDE and J+PEPTIDE, respectively). Bar, 20 µm.

at ~75 kDa and faintly the band at ~105 kDa, whereas the 40-kDa protein band was absent (Fig. 1B). On closer inspection, the strong ~75-kDa protein band appeared as a complex, closely spaced triplet of bands stretched between 70 and 80 kDa. In addition, in tissue cryosections, the novel antibody stained strongly the BBM of S3 segments in the outer stripe, whereas the capillaries and blood vessels in kidney (Fig. 1B), brain, and heart (not shown) remained unstained. In both cases, the labeled protein bands and immunostaining were blocked after preincubation of the antibodies with the relevant immunizing peptides (cf. data in Ref. 50 and present Fig. 2).

Characterization of the novel rSGLT1-ab in immunochemical studies. Before its use in further studies, the novel rSGLT1-ab was characterized by immunoblotting TCM and BBM preparations from the female kidney outer stripe and small intestine (jejunum) and by immunostaining cryosections of the same organs. As shown in Fig. 2A, in the membranes from the kidney outer stripe, in reducing conditions at different heating temperatures, the antibody consistently labeled three protein bands at ~60 (weak), ~75 (strong), and 105 kDa (faint), whereas in nonreducing conditions, two bands, e.g., the strong 75- and the faint 105-kDa bands, were labeled. In the jejunal BBM in reducing conditions, the novel antibody labeled the bands of ~65 (weak) and ~80 kDa (strong), whereas in nonreducing conditions, only one fat band of ~80 kDa was

labeled. In optimal conditions (no β -ME, 65°C, 15 min), the bands in BBM from both tissues, including the faint 105-kDa band in the renal BBM, were blocked after preincubation of the rSGLT1-ab with the immunizing peptide. In further experiments, the 105-kDa band was proven to be always very weak and similar in TCM and BBM preparations from the kidney cortex and outer stripe of both sexes and independent on various treatments. This band was thus considered to be a contaminating, rSGLT1-unrelated protein that weakly cross-reacted with our novel rSGLT1-ab and was not systematically followed in further studies.

In tissue cryosections in optimal conditions, the antibody strongly stained the apical domain of proximal tubule S3 segments in the outer stripe and jejunum. This staining was abolished after preincubation of the antibody with the immunizing peptide (Fig. 2B). The background staining with the peptide-blocked antibody was not different from the staining observed with the secondary antibody only (data not shown). In the following studies in cryosections of various tissues, the rSGLT1-related immunostaining was always tested without and with the peptide-blocked antibody; in most cases, only the specific, peptide-blockable data are shown.

Distribution of rSGLT1 along the nephron: zonal and sex differences. Figure 3 shows zonal and sex differences in distribution of rSGLT1 in the cells of rat nephron. As shown

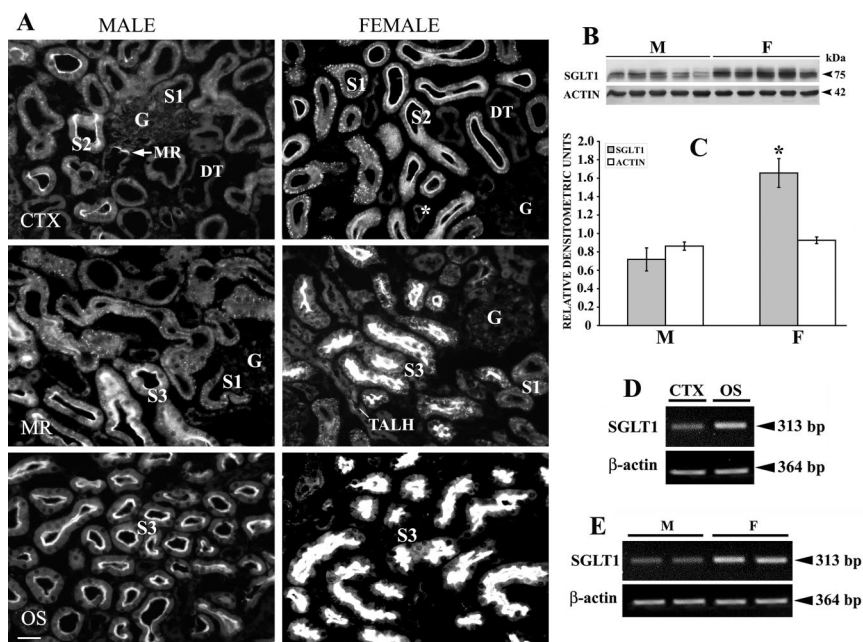


Fig. 3. Distribution of rSGLT1 along the rat nephron: zonal and sex differences. **A:** immunostaining of rSGLT1 in tissue cryosections of the male (M) and female (F) kidneys. In the superficial cortex (CTX) of M kidneys, various proximal tubule profiles were heterogeneously stained: in most tubules, including the initial proximal tubule segment (S1), BBM was not stained, but the cells contained numerous, weakly stained intracellular organelles. The S2 segments exhibited stronger BBM staining and fewer intracellular organelles. The apical domain of macula densa cells (MD) and thick ascending limb of Henle (TALH) (not shown) was weakly stained. The BBM of S3 segments in the medullary rays (MR) and OS were stained more strongly. In F kidneys, the staining intensity of all tubule profiles was stronger than in M kidneys; in the CTX, most S1 segments exhibited a negative to weak BBM staining, and a lot of positively stained intracellular organelles localized largely at the basal pole of the cells. The S2 segments had more strongly stained BBM and fewer intracellular organelles, whereas the BBM of S3 segments in the MR and OS exhibited brightly stained BBM and fewer intracellular organelles. The luminal membrane of the MD (not shown) and TALH was weakly stained. In both sexes, glomeruli (G), distal tubules (DT), and collecting ducts (not shown) were negative. All localizations remained unstained following incubation with the peptide-blocked rSGLT1-ab or with the secondary antibody only (data not shown). Bar, 20 μ m. **B** and **C:** in an immunoblot of BBM isolated from the whole kidneys (**B**) and by densitometric evaluation of the same bands (**C**), the rSGLT1-related 75-kDa protein band was ~130% stronger in F (* P < 0.05 vs. M), whereas the α -actin protein band (42 kDa) showed no sex difference. Each lane in **B** represents the membrane preparation from a separate animal and contained 40 μ g protein. **D:** by RT-PCR, the expression of rSGLT1 mRNA in the renal OS in F was stronger than in M, whereas the expression of β -actin mRNA was similar in both sexes. **E:** in the OS, the expression of rSGLT1 mRNA in F was stronger than in M, whereas mRNA for β -actin showed no sex difference.

in Fig. 3A, in kidneys of adult male and female rats, the rSGLT1-ab stained with variable intensity the BBM and intracellular organelles in proximal tubule epithelial cells and the apical domain of macula densa and cortical thick ascending limb of Henle (TALH; cf. Fig. 4 for details). Other renal structures in the cortex, including renal capsula, glomeruli, other nephron segments, peritubular capillaries, and blood vessels, were not stained (data not shown). In both sexes, the intensity of proximal tubule staining increased toward S3 segments, thus exhibiting segmental $S1 < S2 < S3$ and zonal (cortex $<$ outer stripe) differences. The staining was stronger in females in all proximal tubule segments, confirming the presence of sex differences (male $<$ female). However, a relatively weak staining intensity in macula densa and cortical TALH was similar in males and females (data not shown). The immunoblotting data of BBM isolated from the whole kidneys confirmed the presence of sex differences in the abundance of rSGLT1-related 75-kDa protein; the band in females was $\sim 130\%$ stronger than in males (Fig. 3, B and C). Furthermore, the end-point RT-PCR data indicated that zonal (cortex $<$ outer stripe; Fig. 3D) and sex (male $<$ female; Fig. 3E) differences in the rSGLT1 mRNA expression completely correlated with the expression of rSGLT1 protein.

A more detailed staining in the cells along proximal tubule and in macula densa of female kidney was shown in Fig. 4. As mentioned earlier, in various proximal tubule segments the rSGLT1-ab stained BBM and intracellular organelles with segment-dependent distribution and intensity. Many S1 segments exhibited only a strong staining of numerous intracellular organelles that were largely localized to the middle-to-basal region of epithelial cells (Fig. 4A), whereas in other S1 segments, both intracellular organelles and, weakly, the BBM were stained (Fig. 4B). The S2 segments had generally stronger BBM staining and fewer intracellular organelles (Fig. 4C), and the S3 segments in medullary rays had even stronger BBM staining and less intracellular organelles (Fig. 4D), whereas the

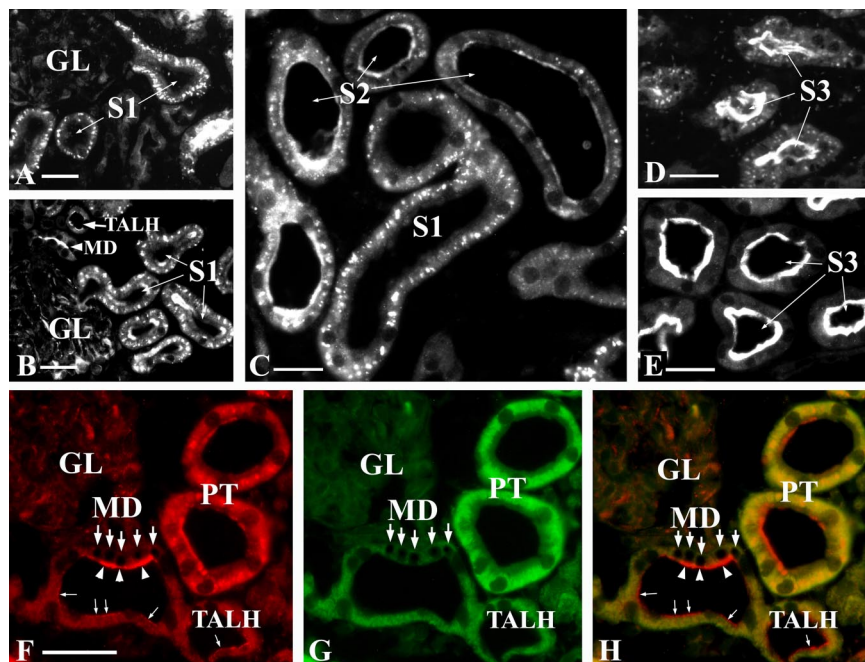
S3 segments in the outer stripe exhibited a brightly stained BBM and absence of intracellular organelles (Fig. 4E).

To better characterize the rSGLT1-positive intracellular organelles, we double-stained cryosections of the female kidney with the rSGLT1-ab and monoclonal or chicken-raised polyclonal antibodies for 1) basolateral membrane (BLM) marker $\text{Na}^+/\text{K}^+-\text{ATPase}$, 2) lysosomal marker LAMP1, 3) mitochondrial marker Ox-Phos, 4) BBM marker NHE3, 5) BBM and endosomal marker megalin, and 6) V-ATPase (31-kDa subunit), a protein localized to the BBM, endocytic vesicles, and other intracellular vacuoles. None of the tested markers showed clear colocalization with the rSGLT1-positive organelles (data not shown).

Figure 4, F–H, shows the rSGLT1-related staining in the macula densa and cortical TALH in female kidney; a relatively weak immunoreactivity was localized to the apical domain of macula densa cells and of the cells in adjacent cortical parts of TALH. However, the parts of TALH in the inner and outer stripe were not stained (data not shown).

Effect of gonadectomy. Animals from both sexes were sham-operated or gonadectomized at the age of 6 wk and killed 6 wk later to perform immunochemical studies in tissue cryosections and isolated membranes. As shown in Fig. 5A, rSGLT1-related immunostaining in the kidney of sham-operated rats was weak in all proximal tubule profiles localized in the cortex, medullary rays, and outer stripe but exhibited the usual pattern of staining intensity, e.g., $S1 < S2 < S3$. In castrated males, the staining intensity increased in all proximal tubule profiles, with the same pattern. In sham-operated females, the intensity of staining along the proximal tubule was stronger than in sham-operated males and remained unchanged after ovariectomy. The effects of gonadectomy were confirmed in Western blotting experiments by testing the abundance of rSGLT1 protein in TCM from the outer stripe; as shown in Fig. 5, B and C, the abundance of rSGLT1-related 75-kDa protein band in the membranes from castrated males was $\sim 100\%$ higher than that

Fig. 4. A–E: rSGLT1 in various proximal tubule segments of the F kidney: correlation between the abundance of intracellular organelles and intensity of brush-border staining. In the cortex, S1 segments exhibited either strong staining of numerous intracellular organelles localized largely in the basal region of epithelial cells, without the BBM staining (A), or weak BBM staining and fewer intracellular organelles (B). In the subcapsular cortex (C), rSGLT1 was present in the S1 segments mostly in numerous intracellular vesicles, whereas the S2 segments exhibited a limited BBM staining and fewer intracellular organelles. In the MR (D), the S3 segments had strong BBM staining and a few intracellular organelles, whereas in the OS (E), the S3 segments exhibited the strongest BBM staining and no intracellular organelles. F–H: detailed localization of the rSGLT1-related staining in MD and TALH in F kidney. rSGLT1-related red fluorescence staining (F) and green fluorescence of the same region showing tissue morphology (G) in a merged image (H) indicate localization of the transporter in the apical domain of MD cells (arrowheads) and TALH (thin arrows). All localizations remained unstained following incubation of cryosections with the peptide-blocked rSGLT1-ab (data not shown). GL, glomerulus; PT, proximal tubule. Large arrows indicate nuclei of MD cells. Bars, 20 μm .



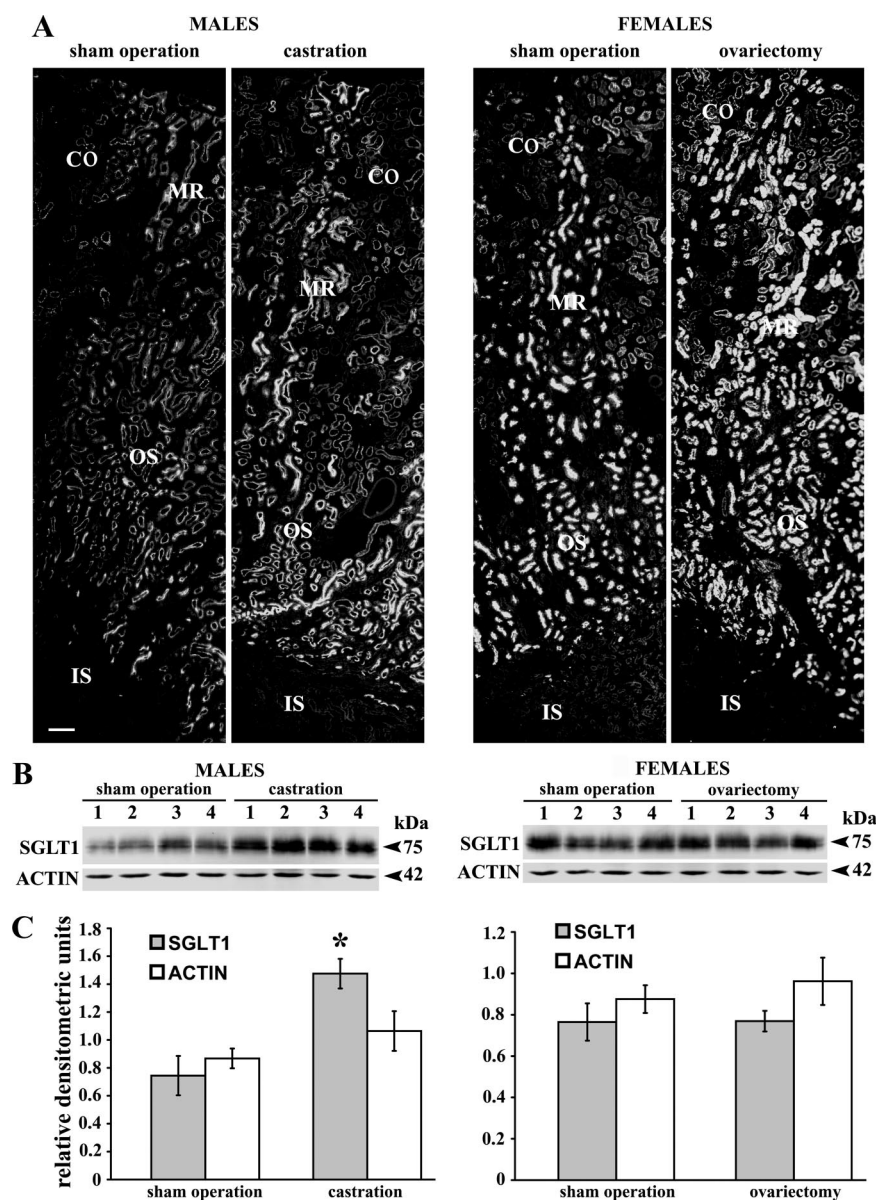


Fig. 5. Effect of gonadectomy on rSGLT1 protein expression along the proximal tubule in M and F kidneys: a view of immunostaining through various tissue zones, Western blots, and densitometric data of the labeled bands in TCM from the OS. *A*: rSGLT1-related staining intensity in all proximal tubule profiles in the renal cortex (CO), MR, and OS was weak in sham-operated M and strong in sham-operated F. In castrated M, the staining intensity increased in all proximal tubule profiles, whereas in ovariectomized F, the staining intensity was not visibly changed. IS, inner stripe (without staining). Bar, 100 μ m. *B*: Western blots of TCM isolated from the OS. *C*: densitometric evaluation of the labeled bands in *B*. The abundance of rSGLT1-related 75-kDa protein band was strongly upregulated in castrated adult M and remained unaffected in ovariectomized adult F, whereas the abundance of α -actin remained unchanged after gonadectomy in both sexes. Each lane contained 60 μ g of protein from a separate TCM preparation. * $P < 0.05$ vs. rSGLT1 in sham-operated M.

from sham-operated males, whereas the abundance in the membranes from sham-operated and ovariectomized females was similar.

Expression of rSGLT1 protein in prepubertal rats. The expression of rSGLT1 protein in prepubertal rats was tested in 20-day-old rats of both sexes by immunocytochemistry in tissue cryosections of the outer stripe and by Western blotting of isolated TCM from the whole kidneys. In both cases, the data from prepubertal rats were compared with the data from one adult female (immunostaining) and from TCM isolated from the whole kidney of one adult female (immunoblotting). As shown by immunostaining (*A*) and Western blotting data (*B* and *C*) in Fig. 6, compared with the data in an adult female, the transporter expression in prepubertal male and female animals was 75% lower and similar in both sexes.

rSGLT1 protein expression in the small intestine of male and female rats. As shown in Fig. 7*A*, in cryosections of the female duodenum, jejunum, and ileum, the rSGLT1 immunoreactivity

was localized strongly to the apical domain of intestinal villi, where it showed regional differences in intensity: jejunum > duodenum = ileum. In all three regions, the staining intensity was weaker at the bottom and increased toward the tip of villi. The double-staining experiments for rSGLT1 and Na^+/K^+ -ATPase, where the primary and secondary antibodies were applied in different sequences (Figs. 7*B* and 8) also showed that 1) rSGLT1 was localized to the BBM of absorptive cells along the entire small intestine with a staining intensity sequence of jejunum > duodenum = ileum; 2) the Na^+/K^+ -ATPase was localized to the BLM of the same cells with the staining intensity increasing toward ileum; 3) the tissue exhibited no false-positive staining with the use of only the secondary antibodies; and 4) the mucus-secreting goblet cells were negative for rSGLT1. The immunoblots of BBM isolated from duodenum, jejunum, and ileum (Fig. 7*C*) and densitometric evaluation of the labeled rSGLT1-related ~80-kDa protein band (Fig. 7*D*) showed that the transporter abundance in

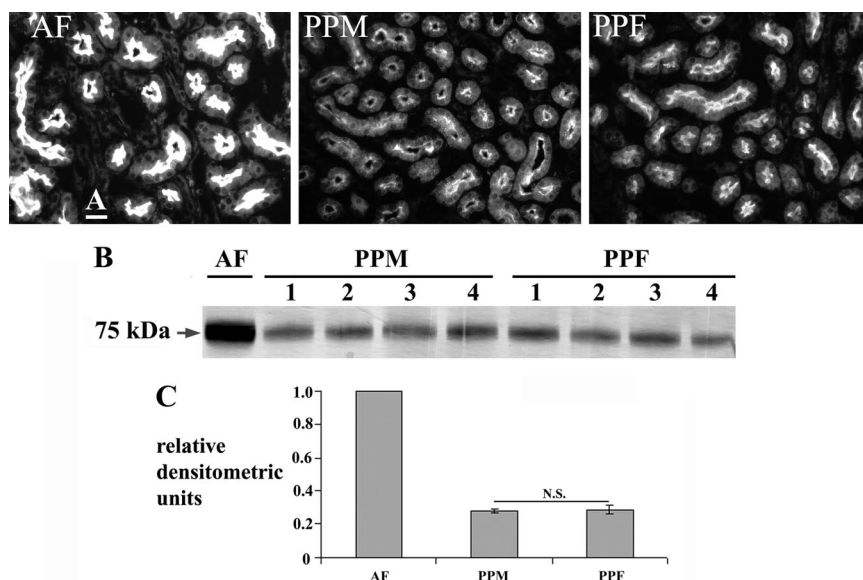


Fig. 6. Expression of renal rSGLT1 protein in an adult F (AF) and in prepubertal M (PPM) and F (PPF) rats. *A*: immunostaining of proximal tubule S3 segments in cryosections of the OS. *B*: immunoblotting of TCM from the whole kidneys. *C*: densitometric evaluation of the labeled protein bands in *B*. The staining intensity in tissue cryosections and the labeling intensity of the rSGLT1-related 75-kDa protein band in PPM and PPF were weak and similar, and were much weaker than in AF. The immunostaining was absent following incubation of cryosections with the peptide-blocked rSGLT1-ab or with the secondary antibody only (data not shown). Bar, 20 μ m. In the Western blot, each lane contained 80 μ g of protein from a TCM preparation from a separate animal.

isolated membranes followed the immunocytochemical pattern of regional differences (jejunum > duodenum = ileum), but sex differences were absent (Fig. 7C).

In addition to the strong staining of BBM in reabsorptive cells, a faint apical staining in the crypts of all three small intestinal regions also was observed, whereas the smooth muscles, capillaries, and other blood vessels remained unstained (Fig. 7A). At a lower concentration of rSGLT1-ab (1:2,000–1:1,000), the staining intensity in the crypts varied in different animals of both sexes and was even absent in some animals, but at higher antibody concentration (1:500–1:200), the apical membrane in the crypts of all regions was clearly positive. A more detailed staining in the jejunal crypts is visible in Fig. 9A (arrows). Furthermore, occasional cells in the crypt epithelium (Fig. 9B, arrowheads) and in villous epithelium (Fig. 9C, arrowhead) in all three intestinal regions were strongly positive for rSGLT1, exhibiting a granular pattern of the staining predominantly localized in the cell basal pole. Various images of these cells that seem to be randomly scattered in the crypt and villous epithelium of all three small intestinal regions are shown in Fig. 10. Finally, the myenteric (Auerbach) plexus between the circular and longitudinal layers of the external musculature was also stained with the rSGLT1-ab (Fig. 9B). With the peptide-blocked rSGLT1-ab, the staining in crypts, myenteric plexus, and villous epithelium was abolished (Fig. 9, D and E).

Immunolocalization of rSGLT1 in the rat stomach and colon. To demonstrate the organ specificity, we tested our novel rSGLT1-ab using immunocytochemical methods in the rat stomach and colon, where the presence of glucose transporters was not to be expected (Fig. 11). The Western blotting of TCM from the stomach and colon mucosa showed that the specific 75-kDa protein band could not be demonstrated in the membranes from both sources (Fig. 11, WB). Furthermore, by immunocytochemistry (Fig. 11, IC), various cells in the stomach (arrowheads) and colon mucosa exhibited a limited and similar autofluorescence when incubated with the rSGLT1-ab (Fig. 11, IC, A) or with the peptide-blocked antibody (Fig. 11, IC, B), but the specific rSGLT1-related immunostaining was not ob-

served. However, the myenteric plexus in the muscularis externa of both organs was brightly stained (Fig. 11, IC, C, arrows), and this staining was blocked by the immunizing peptide (Fig. 11, IC, D, arrows).

Immunolocalization of rSGLT1 in brain, salivary gland, and liver. The novel rSGLT1-ab was further tested by immunocytochemistry in the rat brain, salivary (submandibular) gland, and liver (Fig. 12). In the brain, the staining was weak in pyramidal cells of the cortex (Fig. 12A) and intracellular organelles of individual cells in choroid plexus epithelium (Fig. 12B) and strong in ependymal epithelium (Fig. 12C). The nerve fibers and brain capillaries, which were previously stained with the old antibody in rats and pigs (17, 46), were not stained with the novel antibody (data not shown). In the submandibular gland, the apical domain of initial (intercalated) ducts in serous acini was strongly stained (Fig. 12, D and E), whereas in the liver, the apical domain of bile ducts was strongly stained (Fig. 12, F and G). In addition, unlike previous findings with the old antibody (18), we did not observe staining of capillaries in the heart and skeletal muscles or in aortic endothelium (data not shown).

DISCUSSION

In this study we characterized an improved polyclonal, anti-peptide antibody against the COOH-terminal domain of rSGLT1 by Western blotting and immunocytochemistry in various rat organs. In Western blots under optimal (nondenaturing) conditions, the antibody labeled only one significant, peptide-blockable protein band of ~75 kDa in the renal and ~80 kDa in the small intestinal membranes, both sizes being in the range (72–80 kDa) of previous findings in various animal and human organs and cultured cells (Refs. 17, 18, 32, 46, 50, 52, 59 and references therein). The complexity of these bands, manifested by the closely spaced triplet, most probably reflects different glycosylation states of the protein. In denaturing conditions, however, and in both cases, the antibody labeled two protein bands, one at 75–80 kDa (stronger) and another at 65 kDa (weaker), obviously due to splitting of the holoprotein

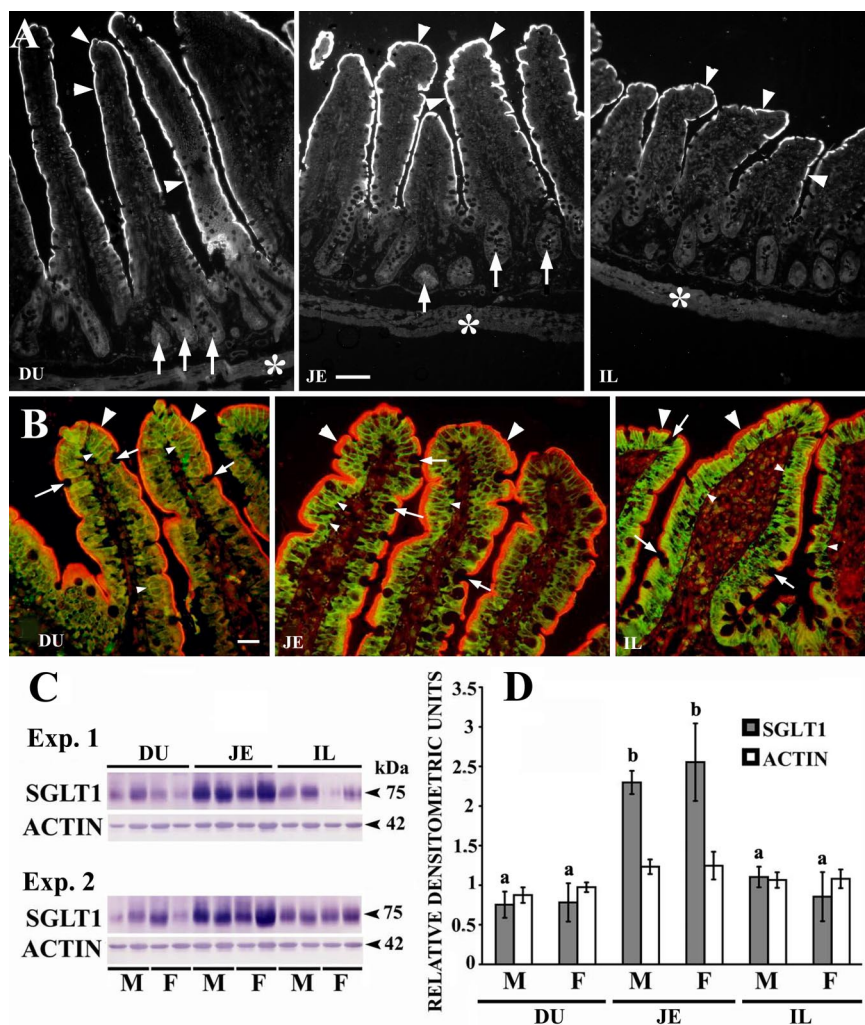


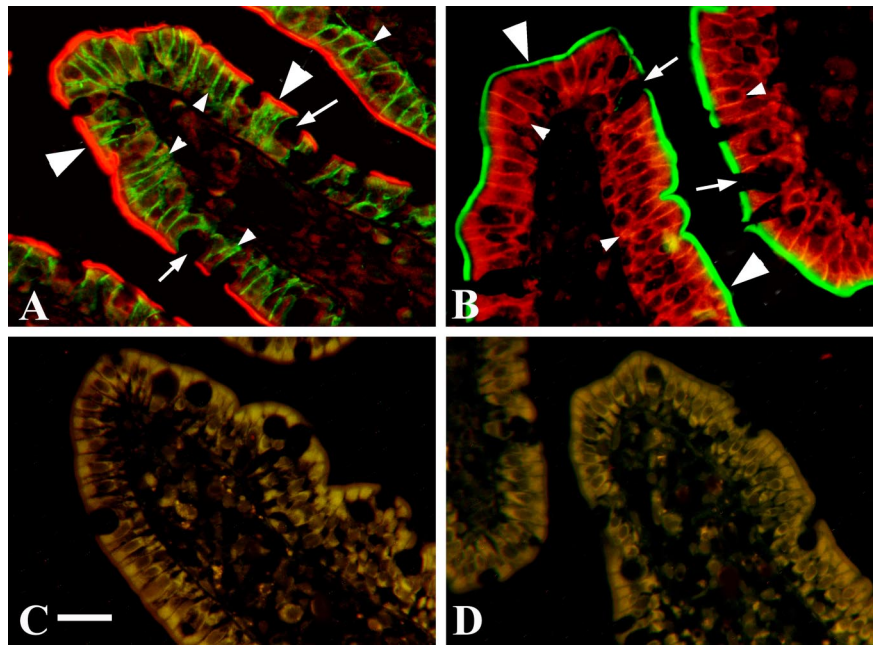
Fig. 7. Regional and sex differences in the rSGLT1 protein expression in small intestine. *A*: immunostaining of rSGLT1 in duodenum (DU), jejunum (JE), and ileum (IL). The transporter was localized strongly to the apical domain of the intestinal villi (arrowheads), exhibiting regional differences in the intensity (JE > DU = IL). The staining intensity was weak at the bottom of villi and increased toward the tip. The apical domain of crypts in DU and JE (arrows), but not in IL, was also faintly stained, whereas the smooth muscles (asterisks) and other structures remained unstained. *B*: double staining for rSGLT1 (red fluorescence) and Na⁺/K⁺-ATPase (green fluorescence) indicated that rSGLT1 was localized to the BBM of absorptive cells (large arrowheads), whereas the goblet cells were negative (thin arrows). The Na⁺/K⁺-ATPase was localized to the cell basolateral membrane (BLM; small arrowheads) and also exhibited regional differences in intensity: DU < JE < IL. Bar, 20 μm. In immunoblots of BBM isolated from DU, JE, and IL of 4 adult M and F rats (*C*) and by densitometric evaluation of the labeled rSGLT1-related ~80-kDa protein band (*D*), the abundance of the transporter exhibited regional (JE > DU = IL) but not sex differences. The α-actin protein band (42 kDa) was similar and sex-independent in all regions. Each lane contained 40 μg of protein. The α-actin band showed no regional differences. ^{a,b}*P* < 0.05 (different letters indicate a significant difference).

(75–80 kDa) into one larger segment that retained the antibody binding epitope (65 kDa) and one or more smaller segments from the NH₂-terminal domain, which was(were) thus not recognized by the rSGLT1-ab. A similar, reducing condition-driven splitting of the holoprotein was recently observed for the organic anion transporter rOat2 protein in the rat kidney (36). The novel rSGLT1-ab, however, did not label the 40-kDa protein band in the renal and intestinal membranes, which was previously identified with our old antibody (50). Therefore, the first three critical amino acid residues (EED), removed from the old immunogen (19-meric peptide), enabled us to generate a more specific antibody that did not recognize the 40-kDa protein band, which most probably came from the CAR-LMPs and did not exhibit the related nonspecific immunostaining. Accordingly, the novel rSGLT1-ab did not stain capillaries and a variety of other structures that had been stained with our old antibody (50). These findings indicate that some previously demonstrated localizations of SGLT1 may be attributed to the cross-reactivity of the antibody with the CAR-LMPs. However, the localization of SGLT1 in endothelial cells of cerebral, renal, coronary, and mesenteric small arteries in rats also has been described in some other studies with different antibodies (20, 21), thus leaving the presence or absence of this glucose transporter in the vascular bed of different rat organs still

questionable. On the other hand, consistent with the findings in previous studies (17, 18, 44, 46, 50, 52), our immunostaining experiments with the novel antibody confirmed the presence of rSGLT1 protein in 1) epithelial cells of the rat nephron, 2) absorptive cells of the small intestine, 3) pyramid cells of the brain cortex, 4) choroid plexus epithelium (in an intracellular compartment), and 5) ependymal epithelium in the brain lateral ventricles. In addition, our new rSGLT1-ab also stained a few, thus far unrecognized localizations of this transporter, such as 1) macula densa cells, 2) epithelium of the cortical TALH, 3) luminal membrane of the initial duct epithelium in the submandibular gland, 4) luminal membrane of the bile duct epithelium, 5) individual cells in the intestinal crypts and villi, and 6) myenteric plexus in the small intestine.

In kidneys, we confirmed our previous findings (50) of zonal (cortex < outer stripe) and sex (female > male) differences in the rSGLT1 expression at the level of protein by immunocytochemistry and immunoblotting. These differences in protein expression matched the pattern of mRNA expression determined by end-point RT-PCR, thus confirming our previous Northern blotting data. In addition, castration upregulated, whereas ovariectomy had no effect on, rSGLT1 protein expression, whereas the prepubertal rats had low and sex-independent expression of rSGLT1 protein in their renal membranes. The

Fig. 8. Efficiency of the primary and secondary antibodies in colocalization studies with rSGLT1-ab and Na/K-ATPase-ab in cryosections of the rat jejunum. The incubation details are described in MATERIALS AND METHODS. *A* and *B*: the SGLT1-ab was applied first and labeled with GARC3 (red); the Na/K-ATPase-ab was applied second and labeled with GARF (green) (*A*), or the Na/K-ATPase-ab was applied first and labeled with GARC3 (red), whereas the rSGLT1-ab was applied second and labeled with GARF (green) (*B*). Either way, the rSGLT1 was localized to the reabsorptive cell BBM (large arrowheads), whereas the Na⁺/K⁺-ATPase was localized to the cell BLM (small arrowheads), without significant overlapping. The goblet cells are indicated by small arrows. *C* and *D*: incubations with only the secondary antibodies, using the same incubation conditions, orders of application, and incubation times as in *A* and *B*, respectively. Except for a limited background staining, no specific staining of the luminal and contraluminal membranes was observed. Bar, 20 μm.

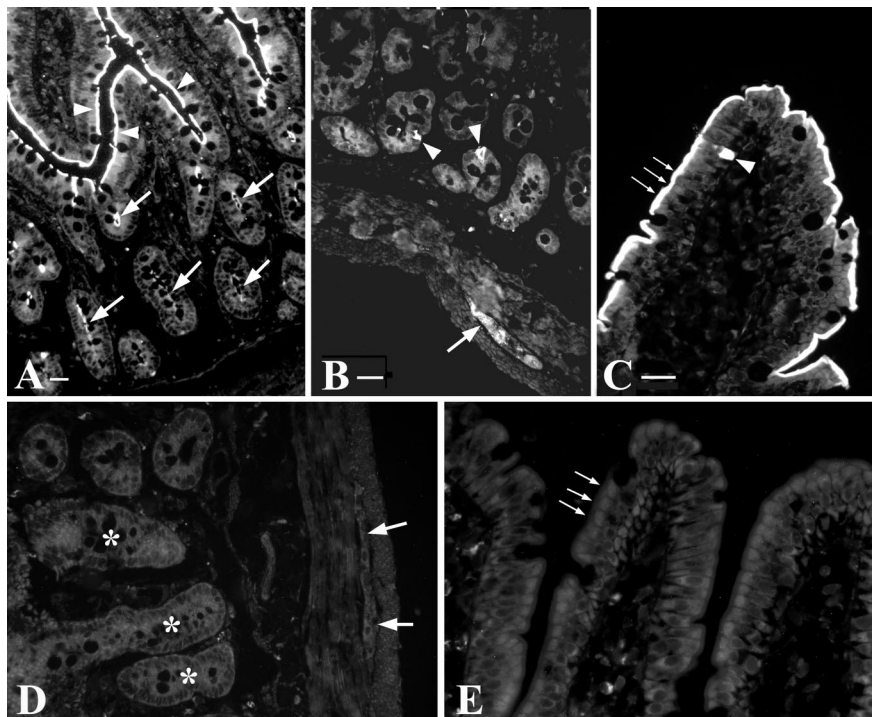


latter data thus confirm our previous conclusions that sex differences (female > male) in the expression of rat renal SGLT1 were determined by the inhibitory action of androgens after puberty (50). However, the missing effects of ovariectomy in adult females (Ref. 50 and this study) and of estrogen and progesterone treatment in castrated rats (50), as well as much lower expression of the transporter in prepubertal females compared with that in an adult female (this study), indicate that the inhibitory action of androgens cannot be the sole regulator (depressor) of the renal rSGLT1 expression, causing sex differences. Some other mechanisms, possibly

growth hormone or some other hormones, or a combination of different hormones, may stimulate the rSGLT1 expression in females after puberty.

The immunostaining in adult rats revealed that, similar to the data described by Takata et al. (52), the rSGLT1 protein was localized in all proximal tubule segments but with a distinct, segment-dependent distribution ratio between the BBM and some intracellular organelles. Whereas the immunoreactivity in BBM increased in intensity from the S1 (negative or weak) toward the S3 segments (strong), the abundance of intracellular organelles decreased from the S1 (many brightly stained or-

Fig. 9. The rSGLT1-related immunostaining and peptide block of the staining in the crypts and myenteric plexus of jejunum. *A*: the BBM in reabsorptive cells was strongly stained (arrowheads), whereas the apical domain in crypts was weakly stained (arrows). *B*: the rare individual cells in the crypt epithelium (arrowheads), as well as the cells of myenteric (Auerbach) plexus in muscularis externa (arrow), were also positive. *C*: the occasional cells in the villous absorptive epithelium (arrowhead) were largely stained at their basal pole with the intensity that was weaker than or similar to that in BBM of reabsorptive cells (thin arrows). *D* and *E*: after incubation of cryosections with the peptide-blocked rSGLT1-ab, the staining in crypts (asterisks) and myenteric plexus (large arrows) (*D*), as well as in the villous epithelium (*E*, small arrows) was absent. Incubation with only the secondary antibody gave no staining as well (data not shown). Bars, 20 μm.



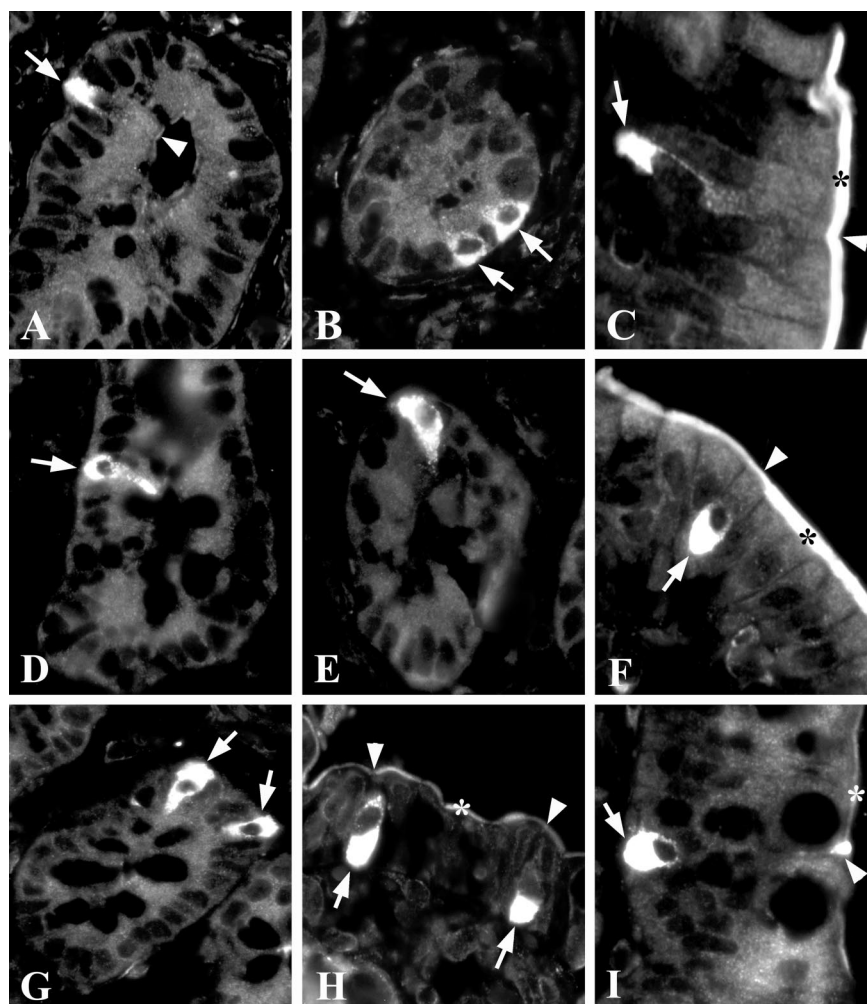


Fig. 10. Various images of the individual rSGLT1-positive cells within the crypt (A, B, D, E, and G) and villous epithelium (C, F, H, and I) in the duodenum (A–C), jejunum (D–F), and ileum (G–I). These cells contained numerous rSGLT1-positive intracellular organelles largely concentrated at the basal pole (arrows), whereas some of them exhibited a variable staining at the luminal membrane (A, C, F, and H, arrowhead). The cells in the ileal epithelium may be connected to the apical surface (asterisk) with a variably long neck (H and I).

ganelles) toward the S3 (absence of organelles). Double-labeling experiments showed that the rSGLT1-positive organelles were negative for various markers for BBM, BLM, and some other known intracellular organelles, but we cannot exclude the possibility that they contain some of the tested markers in a very low concentration. They also cannot represent glycogen granules, because similar structures were not observed in the liver cells. Similar SGLT1-positive intracellular organelles/vesicles were previously described in Caco-2 cells, a culture cell model for human enterocytes (31, 32). In LLC-PK1 cells, a cell line from the pig kidney proximal tubule, the SGLT1-related immunoreactivity was detected beneath the apical membrane (30), whereas in an early immunogold labeling study with several monoclonal antibodies generated against various rSGLT1 epitopes, gold particles were observed over BBM, apical endocytic vacuoles, apical dense tubules, and lysosomes in the rat renal proximal tubules (25). Our data indicate that the rSGLT1 molecules in intracellular organelles and BBM in proximal tubule cells may be in an inverse correlation regarding distribution; the organelles may represent a vesicular reserve pool (storage) of transporters, which may recycle between this compartment and BBM. Analogously with the data in Caco-2 cells expressing human SGLT1 (31), in *Xenopus* oocytes expressing rabbit SGLT1 (27), and in jejunal enterocytes in rats *in vivo* (8), this intracellular pool of vesicles

may possibly regulate the abundance of rSGLT1 in and the transport capacity of the BBM for hexoses in the proximal tubule cells by exo- and endocytosis. In enterocytes, the recycling processes can be modulated by glucose, hormones, and/or other compounds via intracellular signaling and protein kinase-mediated processes (8, 27, 31), but similar phenomena in the proximal tubule cells have not been reported thus far. At this point it is worth mentioning our unexpected finding of the rSGLT1 immunoreactivity in the apical domain of macula densa cells. SGLT1 in these cells may represent the uptake mechanism for glucose as an energy donor, but it also may serve as a sensor of the residual (unreabsorbed) glucose/galactose in the luminal fluid. The cells may sense the local hexose concentration and react by some neural and/or humoral messages that could affect the abundance of SGLT1 molecules in the BBM by changing the intracellular trafficking of transporter-containing vesicles and accordingly change the capacity of hexose reabsorption in proximal tubules.

In the small intestine, the rSGLT1 protein was strongly expressed in the BBM of absorptive cells, more in those at the villi tip, and weakly in the apical membrane of crypt cells. The observed increasing staining intensity from the bottom toward the tip of villi in all three small intestinal regions in rats is at variance with the previously described *in situ* hybridization data, which localized the rSGLT1 mRNA predominantly in the

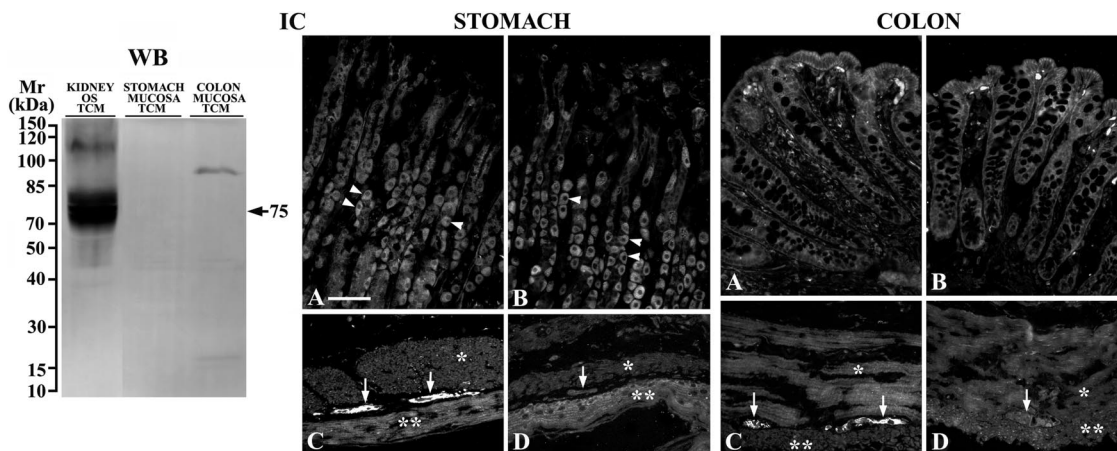


Fig. 11. Immunolocalization of rSGLT1 in the rat stomach and colon. *Left*, Western blot (WB) of TCM from the kidney cortex OS and of stomach and colon mucosa with the rSGLT1-ab. The rSGLT1-related 75-kDa protein band was strong in the renal TCM and negative in TCM prepared from the stomach and colon mucosa. In the colonic membranes, only a protein band at ~95 kDa was faintly labeled. *Right*, immunoreactivity in cryosections (immunocytochemistry, IC) of the stomach and colon mucosa (A and B) and muscularis externa (C and D) with the rSGLT1-ab (A and C) or the peptide-blocked antibody (B and D). In the stomach mucosa (A and B), the oxyntic cells exhibited a significant autofluorescence (arrowheads), but a specific rSGLT1-related staining was not observed in any cell type. The overall weak staining with the native and peptide-blocked antibody was similar and reflected the background staining that was also present after only the secondary antibody was used (data not shown). In the muscularis externa (C and D), the myenteric plexus between the circular (single asterisk) and longitudinal (double asterisk) muscle layers was brightly stained (C, arrows); this staining was blocked by the immunizing peptide (D, arrow). In the colon mucosa, only a weak background staining with the native (A) and peptide-blocked rSGLT1-ab (B) was recorded. This background staining was also present after only the secondary antibody was used (data not shown). However, a clear staining of myenteric plexus in the muscularis externa (C, arrows) was blocked by the immunizing peptide (D, arrow). Bar, 50 μ m.

absorptive cells lining the lower two-thirds of the villi but showed its absence in crypts (34). The absence of both SGLT1 mRNA and protein in crypts was also described in rabbits (29), whereas the immunoreactivity with monoclonal antibodies was previously demonstrated in crypts of all three intestinal regions in rats (24). In accordance with the previous transport, immunohistochemical (with monoclonal antibodies), and *in situ* hybridization data (15, 24, 34), we presently confirmed segmental differences in the abundance of rSGLT1 protein along the small intestine in adult rats, with the highest being in jejunum. In both male and female rats, the abundance of rSGLT1 protein in the jejunal BBM was approximately threefold above that in duodenum and ileum, thus indicating jejunum as the sex-independent, major place of sugar absorption in the intestine. As expected, the rSGLT1 protein was not detected in the cells of stomach and colon mucosa, thus proving 1) an insignificant role of these two parts of the mammalian gastrointestinal tract in sugar reabsorption and 2) that our new rSGLT1-ab stained only specific localizations of this transporter.

In addition to the reabsorptive cells, a clear rSGLT1-related immunoreactivity was detected in the apical domain and intracellular organelles in the individual cells that were randomly scattered among the epithelium of crypts and villi in all three small intestinal segments. The nature of these cells is not known. They cannot be the Paneth cells, which reside exclusively at the crypt bottom. Rather, they may represent a thus far unrecognized subpopulation of the randomly scattered neuroendocrine (chemosensory) cells in the sugar-absorptive intestinal epithelium that may sense the local concentration of hexoses. They may behave as a kind of sweet taste receptors, which may be activated by the intestinal glucose and produce locally acting (paracrine) hormones. These hormones may activate or inhibit the intracellular signaling-mediated (via protein kinases and regulatory protein RS1) endo- and exocytosis of the transporter-carrying intracellular recycling vesicles.

Thus regulated abundance of SGLT1 in the enterocyte BBM may contribute to the well-known rapid adaptation of sugar transport in the mammalian small intestine (8, 12, 27, 28, 39, 40, 57). Furthermore, a limited immunostaining of myenteric plexus (Auerbach) in the muscularis externa indicates that these cells contain SGLT1 in addition to previously demonstrated SGLT3 (*Slc5a4*) (14). Since SGLT3 was shown to be a glucose sensor rather than a glucose transporter, SGLT1 in the myenteric plexus may principally provide metabolic fuel to these cells. However, since it is present in the muscularis externa of both sugar absorptive (small intestine) and nonabsorptive (stomach, colon) segments, contribution of the myenteric SGLT1 to a hexose-dependent reflex regulation of the intestinal peristalsis and secretion cannot be excluded for now.

Our finding of rSGLT1 immunoreactivity in the apical domain of liver bile ducts and initial (intercalated) ducts of submandibular gland merits a sensible attention. Previous studies demonstrated that in physiological conditions in rats, but not in humans, glucose is secreted into the bile by the liver cells by an unknown mechanism and then partially (re)absorbed along the biliary ducts, thus serving bilihepatic circulation of glucose (9, 23, 33, 41). As estimated in the *in situ* microperfused bile duct in rats, the rate of glucose transport (absorption) in these ducts matched the rate measured in microperfused proximal convoluted tubules of the rat and rabbit kidneys (41). In normal rats, the concentration of glucose in bile was estimated to be up to 30% (1–2 mM) of that in blood plasma (5–6 mM); it increased in the presence of the SGLT1 inhibitor phlorizin, and in the same time, the bile flow increased (9, 23). On the other hand, with more glucose in bile (absence of phlorizin), the (re)absorption of water increased, resulting in lower bile flow (35). Previous studies in rat liver demonstrated 1) phlorizin-sensitive Na^+ -monosaccharide cotransport in the apical membrane of cultured cholangiocytes, 2) SGLT1 mRNA by Northern blot analysis in the liver tissue

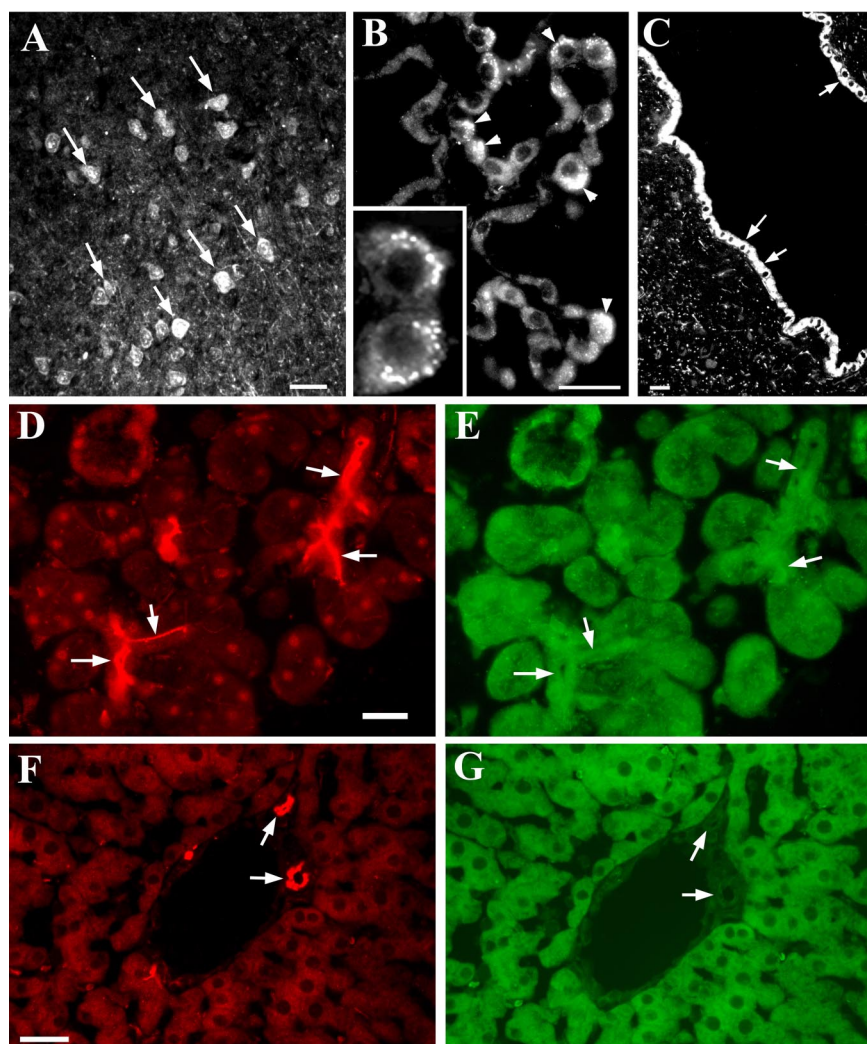


Fig. 12. rSGLT1-related immunostaining in the brain (A–C), submandibular salivary gland (D and E), and liver (F and G). In the brain, pyramidal cells in the brain cortex (A, arrows), intracellular organelles in individual cells of the choroid plexus epithelium (B, arrowheads and *inset*), and ependymal epithelium (C, arrows) were stained. In the submandibular gland, the apical domain of initial ducts in serous acini (D, arrows) was strongly stained; the green image (E) shows morphology of the same region. In the liver, the apical domain of bile ducts (F, arrows) was strongly stained; the green image shows morphology of the same region and bile ducts (G, arrows). The immunostaining was absent following incubation of cryosections with the peptide-blocked rSGLT1-ab or with the secondary antibody only (data not shown). Bars, 20 μ m.

and by RT-PCR in freshly isolated cholangiocytes, and 3) SGLT1 mRNA by in situ RT-PCR exclusively in bile duct cells (33, 34). Therefore, our immunocytochemical finding of the rSGLT protein in the apical membrane of bile ducts is a perfect match with the previous transport and mRNA studies. SGLT1 in these ducts may play a crucial role in regulating ductal bile formation and concentration; glucose reabsorption via SGLT1 may provide a driving force for a direct Na^+ , glucose, and water cotransport or/and may generate a critical osmotic driving force for water transport via water channels localized to the bile duct apical (aquaporin-1; AQP1) and basolateral (AQP4) membranes (38, 41, 42, 49, 51). The reabsorbed glucose may exit the cells via the basolaterally localized glucose facilitator GLUT1 (33).

The localization of rSGLT1 protein to the apical domain of initial (intercalated) ducts in submandibular gland is in contradiction with the previously described localization of this transporter to the BLM of acinar cells in the rat submandibular gland (18) and sheep parotid gland (53). Although the previous data in rats may be possibly attributed to the use of our old antibody that may have stained CAR-LMP in the plasma membrane of myoepithelial cells and/or capillaries that surround acinar cells, the experiments in sheep parotid gland were performed with a different antibody, which labeled a strong

SGLT1-related 75-kDa protein in isolated BLM from the ovine gland. At the present time, without detailed experimentation we cannot answer whether differences exist in the localization of SGLT1 protein in the acini of parotid and submandibular glands in rats and whether the basolateral localization in the parotid gland acini is specific for ruminants. However, localization of rSGLT1 to the luminal membrane of the initial ducts may be highly relevant to the presence of glucose in saliva, a phenomenon detected 100 years ago by Carlson and Ryan (6) in cats and later confirmed and studied in various (patho)physiological conditions in humans (1, 22, 47). Although the exact source of glucose in saliva is not known, it may be isosmotically secreted by serous acini and later largely reabsorbed along the initial ducts by the SGLT1-mediated process similar to that in the small intestine, renal proximal tubules, and liver bile ducts. Accordingly, in the salivary gland initial ducts, glucose transport may contribute to the reabsorption of water, either by simultaneous cotransport with Na^+ and glucose (38) and/or by generating the transmembrane osmotic gradient that drives water movement, possibly through the (still controversial) apically located water channel AQP5 (7, 13, 43). It is, however, unclear how glucose can leave the duct cell at the basolateral membrane; glucose transporters in the mammalian salivary glands have not been systematically studied. If the

primary secretion by acini contains a concentration of glucose similar to that in plasma, the measured glucose in unstimulated mixed saliva in humans (0.02–0.4 mM, 15–300 times less than in the blood plasma, Ref. 22) indicates strong reabsorptive mechanisms along the salivary ducts, most probably by the apically located SGLT1.

In conclusion, in this report we have described the use of an improved polyclonal anti-peptide antibody highly specific for the rat high-affinity Na⁺-glucose cotransporter SGLT1. The antibody may be used to identify novel sites of SGLT1 protein localization in rat organs and to study its expression in various physiological, pathophysiological, and toxicological conditions in the rat kidney, small intestine, and other organs.

ACKNOWLEDGMENTS

We thank Eva Heršak for expert technical assistance.

GRANTS

This work was supported by Ministry for Science, Education and Sports, Croatia Gants 022-0222148-2146 (to I. Sabolić) and Deutsche Forschungsgemeinschaft Grant 487/C1 (to H. Koepsell).

REFERENCES

- Andersson AB, Birkhed D, Berntorp K, Lindgarde F, Matsson L. Glucose concentration in parotid saliva after glucose/food intake in individuals with glucose intolerance and diabetes mellitus. *Eur J Oral Sci* 106: 931–937, 1998.
- Antolovic R, Hamer E, Serpersu EH, Kost H, Linnertz H, Kovarik Z, Schoner W. Affinity labelling with MgATP analogues reveals coexisting Na⁺ and K⁺ forms of the α -subunits of Na⁺/K⁺-ATPase. *Eur J Biochem* 261: 181–189, 1999.
- Barfuss DW, Schafer JA. Differences in active and passive glucose transport along the proximal nephron. *Am J Physiol Renal Fluid Electrolyte Physiol* 241: F322–F332, 1981.
- Biber J, Stieger B, Haase W, Murer H. A high yield preparation for rat kidney brush-border membranes: different behavior of lysosomal markers. *Biochim Biophys Acta* 647: 169–176, 1981.
- Bradford MM. A rapid and sensitive method for the quantitation of microgram quantities of protein utilizing the principle of protein-dye binding. *Anal Biochem* 72: 248–254, 1976.
- Carlson AJ, Ryan JG. Glucose in saliva. *Am J Physiol* 21: 301–309, 1908.
- Charron FM, Blanchard MG, Lapointe JY. Intracellular hypertonicity is responsible for water flux associated with Na⁺/glucose cotransport. *Biophys J* 90: 3546–3554, 2006.
- Cheeseman CI. Upregulation of SGLT-1 transport activity in rat jejunum by GLP-2 infusion in vivo. *Am J Physiol Regul Integr Comp Physiol* 273: R1965–R1971, 1997.
- Crafer SMD, Pryor JS, Dawson AP. Effect of arterial-portal glucose gradients and phloridzin on bile glucose levels in perfused rat liver. *J Physiol* 479: 281–289, 1994.
- Cramer SC, Pardrige WM, Hirayama BA, Wright EM. Colocalization of GLUT2 glucose transporter, sodium/glucose cotransporter, and gamma-glutamyl transpeptidase in rat kidney with double-peroxidase immunocytochemistry. *Diabetes* 41: 766–770, 1992.
- Crljen V, Sabolić I, Susac J, Appenroth D, Herak-Kramberger CM, Ljubojević M, Anzai N, Antolovic R, Burckhardt G, Fleck C, Sabolić I. Immunocytochemical characterization of the incubated rat renal cortical slices. *Pflügers Arch* 450: 269–279, 2005.
- Debnam ES. Rapid adaptation of intestinal sugar transport. *News Physiol Sci* 9: 84–88, 1994.
- Delporte C, Steinfeld S. Distribution and roles of aquaporins in salivary glands. *Biochim Biophys Acta* 1758: 1061–1070, 2006.
- Diez-Sampedro A, Hirayama BA, Osswald C, Gorboulev V, Baumgarten K, Volk C, Wright EM, Koepsell H. A glucose sensor hiding in a family of transporters. *Proc Natl Acad Sci USA* 100: 11753–11758, 2003.
- Dong R, Srail SK, Debnam E, Smith M. Transcriptional and translational control over sodium-glucose-linked transporter (SGLT1) gene expression in adult small intestine. *FEBS Lett* 406: 79–82, 1997.
- Eguchi J, Wada K, Hida K, Zhang H, Matsuoka T, Baba M, Hashimoto I, Shikata K, Pgawa N, Makino H. Identification of adipocyte adhesion molecule (ACAM), a novel CTX gene family, implicated in adipocyte maturation and development of obesity. *Biochem J* 387: 343–353, 2005.
- Elfeber K, Köhler A, Lutzenburg M, Osswald C, Galla HJ, Witte OW, Koepsell H. Localization of the Na⁺-D-glucose cotransporter SGLT1 in the blood-brain barrier. *Histochem Cell Biol* 121: 201–207, 2004.
- Elfeber K, Stümpel F, Gorboulev V, Matting S, Deussen A, Kaissling B, Koepsell H. Na⁺-D-glucose cotransporter in muscle capillaries increases glucose permeability. *Biochem Biophys Res Commun* 314: 301–305, 2004.
- Frigeri A, Gropper MA, Umenishi F, Kawashima M, Brown D, Verkman AS. Localization of MIWC and GLIP water channel homologs in neuromuscular, epithelial and glandular tissues. *J Cell Sci* 108: 2993–3002, 1995.
- Gaudreault N, Scriven DRL, Moore EDW. Asymmetric subcellular distribution of glucose transporters in the endothelium of small contractile arteries. *Endothelium* 13: 317–324, 2006.
- Gaudreault N, Scriven DRL, Moore EDW. Characterisation of glucose transporters in the intact coronary artery endothelium in rats: GLUT-2 upregulated by long-term hyperglycemia. *Diabetologia* 47: 2181–2092, 2004.
- Gough H, Luke GA, Beeley JA, Geddes DAM. Human salivary glucose analysis by high-performance ion-exchange chromatography and pulsed amperometric detection. *Arch Oral Biol* 41: 141–145, 1996.
- Guzelian P, Boyer JL. Glucose reabsorption from bile. Evidence for a biliohepatic circulation. *J Clin Invest* 53: 526–535, 1974.
- Haase W, Heltmann K, Friese W, Ollig D, Koepsell H. Characterization and histochemical localization of the rat intestinal Na⁺-D-glucose cotransport by monoclonal antibodies. *Eur J Cell Biol* 52: 297–309, 1990.
- Haase W, Koepsell H. Electron microscopic immunohistochemical localization of components of Na⁺-cotransporters along the rat nephron. *Eur J Cell Biol* 48: 360–374, 1989.
- Hediger MA, Rhoads DB. Molecular physiology of sodium-glucose cotransporters. *Physiol Rev* 74, 993–1026, 1994.
- Hirsch JR, Loo DDF, Wright EM. Regulation of Na⁺/glucose cotransporter expression by protein kinases in *Xenopus laevis* oocytes. *J Biol Chem* 271: 14740–14746, 1996.
- Hofer D, Asan E, Drenckhahn D. Chemosensory perception in the gut. *News Physiol Sci* 14: 18–23, 1999.
- Hwang ES, Hirayama BA, Wright EM. Distribution of the SGLT1 Na⁺/glucose cotransporter and mRNA along the crypt-villus axis of rabbit small intestine. *Biochem Biophys Res Commun* 181: 1208–1217, 1991.
- Ikari A, Nakano M, Kawano K, Suketa Y. Up-regulation of sodium-dependent glucose transporter by interaction with heat shock protein 70. *J Biol Chem* 277: 33338–33343, 2002.
- Khoursandi S, Scharlau D, Herter P, Kuhnen C, Martin D, Kinne RKH, Kipp H. Different modes of sodium-D-glucose cotransporter-mediated D-glucose uptake regulation in Caco-2 cells. *Am J Physiol Cell Physiol* 287: C1041–C1047, 2004.
- Kipp H, Khoursandi S, Scharlau D, Kinne RKH. More than apical: distribution of SGLT1 in Caco-2 cells. *Am J Physiol Cell Physiol* 285: C737–C749, 2003.
- Lazaridis KN, Pham L, Vroman B, DeGroen PC, LaRusso NF. Kinetic and molecular identification of sodium-dependent glucose transporter in normal rat cholangiocytes. *Am J Physiol Gastrointest Liver Physiol* 272: G1168–G1174, 1997.
- Lee WS, Kanai Y, Wells RG, Hediger MA. The high affinity Na⁺/glucose cotransporter. *J Biol Chem* 269: 12032–12039, 1994.
- Lira M, Schlesinger CD, Steinbach JH, Lambert K, Microburst JA, Hofmann AF. Sugar absorption by the biliary ductular epithelium of the rat: evidence for two transport systems. *Gastroenterology* 102: 563–571, 1992.
- Ljubojević M, Balen D, Breljak D, Susan M, Anzai N, Bah A, Burckhardt G, Sabolić I. Renal expression of organic anion transporter OAT2 in rats and mice is regulated by sex hormones. *Am J Physiol Renal Physiol* 292: F361–F372, 2007.
- Ljubojević M, Herak-Kramberger CM, Hags Y, Bah A, Endow H, Burckhardt G, Sabolić I. Rat renal cortical OAT1 and OAT3 exhibit gender differences determined by both androgen stimulation and estrogen inhibition. *Am J Physiol Renal Physiol* 287: F124–F138, 2004.
- Loo DDF, Wright EM, Heathen T. Water pumps. *J Physiol* 542: 53–60, 2002.

39. Mace OJ, Affleck J, Patel N, Pellet GL. Sweet taste receptors in rat small intestine stimulate glucose absorption through apical GLUT2. *J Physiol* 582: 379–392, 2007.
40. Margolskee RF, Dyer J, Kokrashvili Z, Salmon KSH, Ilegems E, Daly K, Maillet EL, Ninomiya Y, Mosinger B, Shirazi-Beechey SP. T1R3 and gustducin in gut sense sugars to regulate expression of Na⁺-glucose cotransporter 1. *Proc Natl Acad Sci USA* 104: 15075–15080, 2007.
41. Masyuk AI, Masyuk TV, Tietz PS, Splinter PL, LaRusso NF. Intrahepatic bile ducts transport water in response to absorbed glucose. *Am J Physiol Cell Physiol* 283: C785–C791, 2002.
42. Masyuk AI, LaRusso NF. Aquaporins in the hepatobiliary system. *Hepatology* 43: S75–S81, 2006.
43. Nielsen S, King LS, Christensen BM, Agre P. Aquaporins in complex tissues. II. Subcellular distribution in respiratory and glandular tissues of rat. *Am J Physiol Cell Physiol* 273: C1549–C1561, 1997.
44. Pajor AM, Hirayama BA, Wright EM. Molecular evidence for two renal Na⁺/glucose transporters. *Biochim Biophys Acta* 1106: 216–2120, 1992.
45. Pajor AM, Wright EM. Cloning and functional expression of a mammalian Na⁺/nucleoside cotransporter. *J Biol Chem* 267: 3557–3560, 1992.
46. Poppe R, Karbach U, Gambaryan S, Wiesinger H, Lutzenburg M, Kraemer M, Witte OW, Koepsell H. Expression of the Na⁺-D-glucose cotransporter SGLT1 in neurons. *J Neurochem* 69: 84–94, 1997.
47. Prosser CG, Hartmann PE. Saliva and breast milk composition during the menstrual cycle of women. *Aust J Exp Biol Med Sci* 61: 265–275, 1983.
48. Raschperger E, Engstrom U, Pettersson RF, Fuxe J. CLMP, a novel member of CTX family and a new component of epithelial tight junctions. *J Biol Chem* 279: 796–804, 2004.
49. Roberts SK, Yano M, Ueno Y, Pham L, Alpini G, Agre P, LaRusso NF. Cholangiocytes express the aquaporin CHIP and transport water via a channel-mediated mechanism. *Proc Natl Acad Sci USA* 91: 13009–13013, 1994.
50. Sabolić I, Skarica M, Gorboulev V, Ljubojević M, Balen D, Herak-Kramberger CM, Koepsell H. Rat renal glucose transporter SGLT1 exhibits zonal distribution and androgen-dependent gender differences. *Am J Physiol Renal Physiol* 290: F913–F926, 2006.
51. Splinter PL, Masyuk AI, Marinell RA, LaRusso NF. AQP4 transfected into mouse cholangiocytes promotes water transport in biliary epithelia. *Hepatology* 39: 109–116, 2004.
52. Takata K, Kasahara M, Ezaki O, Hirano H. Localization of Na⁺-dependent active type and erythrocyte/HepG2-type glucose transporters in rat kidney: immunofluorescence and immunogold study. *J Histochem Cytochem* 39: 287–298, 1991.
53. Tarpey PS, Wood IS, Shirazi-Beechey SP, Beechey RB. Amino acid sequence and the cellular location of the Na⁺-dependent D-glucose symporters (SGLT1) in the ovine enterocyte and the parotid acinar cell. *Biochem J* 312: 293–300, 1995.
54. Turner RJ, Moran A. Heterogeneity of sodium-dependent D-glucose transport sites along the proximal tubule: evidence from vesicle studies. *Am J Physiol Renal Fluid Electrolyte Physiol* 242: F406–F414, 1982.
55. Turner RJ, Moran A. Further studies of proximal tubular brush border membrane D-glucose transport heterogeneity. *J Membr Biol* 70: 37–45, 1982.
56. Turner RJ, Moran A. Stoichiometric studies of the renal outer cortical brush border membrane D-glucose transporter. *J Membr Biol* 67: 73–80, 1982.
57. Veyhil M, Wagner CA, Gorboulev V, Schmitt BM, Lang F, Koepsell H. Downregulation of the Na⁺-D-glucose cotransporter SGLT1 by protein RS1 (RSC1A1) is dependent on dynamin and protein kinase C. *J Membr Biol* 196: 71–81, 2003.
58. Wells RG, Pajor AM, Kanai Y, Turk E, Wright EM, Hediger MA. Cloning of a human kidney cDNA with similarity to the sodium-glucose cotransporter. *Am J Physiol Renal Fluid Electrolyte Physiol* 263: F459–F465, 1992.
59. Wright EM. Renal Na⁺-glucose cotransporters. *Am J Physiol Renal Physiol* 280: F10–F18, 2001.
60. You G, Lee WS, Barros JG, Kanai Y, Huo TL, Khawaja S, Wells RG, Nigam SK, Hediger MA. Molecular characteristics of Na⁺-coupled glucose transporters in adult and embryonic rat kidney. *J Biol Chem* 270: 29365–29371, 1995.